

Gated Convolutional Networks with Hybrid Connectivity for Image Classification

Chuangang Yang^{1,2}, Zhulin An^{1*}, Hui Zhu^{1,2}, Xiaolong Hu^{1,2},
Kaiqiang Xu^{1,2}, Chao Li¹, Boyu Diao¹, Yongjun Xu¹

¹Institute of Computing Technology, Chinese Academy of Sciences, Beijing, China

²University of Chinese Academy of Sciences, Beijing, China

Abstract

We design a highly efficient architecture called Gated Convolutional Network with Hybrid Connectivity (HCGNet), which is equipped with the combination of local residual and global dense connectivity to enjoy their individual superiorities as well as attention-based gate mechanism to assist feature recalibration. To adapt our hybrid connectivity, we further propose a novel module which includes a squeeze cell for obtaining the compact features from input and then a multi-scale excitation cell attached an update gate to model the global context features for capturing long-range dependency based on multi-scale information. We also locate a forget gate on residual connectivity to decay the reused features, which can be aggregated with newly global context features to form the output that can facilitate effective feature exploration as well as re-exploitation to some extent. Moreover, the number of our proposed modules under dense connectivity can quite fewer than classical DenseNet thus reducing considerable redundancy but with empirically better performance. On CIFAR-10/100 datasets, HCGNets significantly outperform state-of-the-art both human-designed and auto-searched networks with much fewer parameters. It can also consistently obtain better performance and interpretability than widely applied networks in practice on ImageNet dataset.

Introduction

Deep convolutional neural networks (CNNs) are becoming more and more efficient in parameter and computation without sacrificing the performance owing to novel architectures design. ResNet (He et al. 2016) introduces the residual connectivity to implement the addition of the input and output features for each micro-block. DenseNet (Huang et al. 2017) holds the dense connectivity by changing skip connections from addition to concatenation. Both of their feature aggregation connectivities can not only encourage feature reuse, but also ease the training problems. For a comparison, dense connectivity is more effect for feature exploitation and exploration but exists a certain redundancy, while residual connectivity contributes efficient feature reuse by parameter sharing mechansim and thus leads to low redundancy, but lacks the capability of feature preservation and

*Corresponding author
Preprint. Under review.

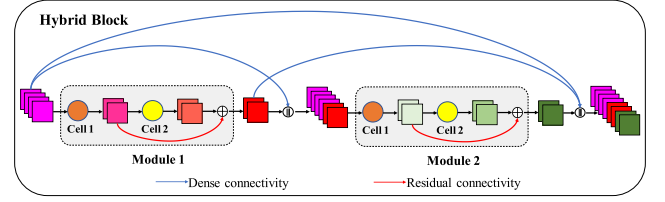


Figure 1: The diagram of a hybrid block including $n = 2$ modules, where $n \geq 2$. The symbol "+" and "||" denote element-wise addition and channel-wise concatenation among multiple feature maps, respectively.

exploration. To enjoy their advantages and avoid inherent limitations, many networks combine them to build a more effective aggeration topology, such as DPN(Chen et al. 2017), MixNet(Wang et al. 2018a) and AOGNet(Li, Song, and Wu 2019). Differ them, we develop a hybrid connectivity (Fig.1) that facilitates feature flow and aggeration by dense connectivity for global channel-wise concatenation of outputs produced by all precedent modules (blue links in Fig.1) and residual connectivity for local element-wise summation within the module (red links in Fig.1).

Our main motivation for this pattern design originates from reducing the redundancy of dense connectivity. As the depth of network linearly increases, the number of skip connections and required parameters grow by a rate of $O(n^2)$, where n denotes the number of stacked modules under dense connectivity. Meanwhile, superfluous features are transferred quadratically to subsequent modules. So one simple method to reduce redundancy is to decrease the number of modules directly, but it can attenuate the representational power of features and then deteriorate the performance. Thus we develop a novel module by embedding the residual connectivity to assist feature learning within the local module. Experimentally, the number of our modules in the hybrid block can be quite fewer than that of classical modules in the dense block but without sacrificing the performance.

For further adaptation with hybrid connectivity, we instantiate the basic module that includes a squeeze cell (cell 1 in Fig.1) for transforming the input to a compact feature

map, and a multi-scale excitation cell (cell 2 in Fig.1) to further extract multi-scale features by multi-kernel convolutions. It is widely known that convolution builds pixel relationship in a local neighborhood, which leads to ineffective modeling of long-range dependency. To fully address this issue, we develop an update gate to model the global context features from more informative multi-scale features. Moreover, we locate a forget gate on the residual connection to capture channel-wise dependency for decaying the reused features produced by cell 1. Finally, global context features are added to the reused feature map of each spatial position to form the output, which can not only promote effective feature exploration but also retain the capability of feature re-exploitation to some extent. Moreover, both forget gate and update gate are lightweight and general plug-ins, which can be integrated into any CNNs with negligible overheads.

To demonstrate the effectiveness and efficiency of our proposed HCGNets, we perform extensive experiments across the three highly competitive image classification datasets: CIFAR-10/100 (Krizhevsky and Hinton 2009), and ImageNet (ILSVRC 2012) (Deng et al. 2009). On CIFAR datasets, HCGNets outperforms state-of-the-art both human-designed and auto-searched networks but only requires extremely fewer parameters, e.g., HCGNet (11.4M) obtains the better results than the most competitive NASNet-A (50.9M) with $4.5\times$ fewer parameters. Moreover, HCGNet (3.1M) achieves above absolute 1.1%/0.4% accuracy gains on CIFAR-10/100 compared with concurrent AOGNet (15.8M), which is the state-of-the-art human-designed combination of ResNet and DenseNet. On ImageNet datasets, it also consistently obtain the best accuracy and interpretability among the widely used networks in practice with less or comparable parameter size and computation.

Related Work

Improvements of ResNet and DenseNet. ResNeXt (Xie et al. 2017) outperforms ResNet with less overheads since it adopts 3×3 group convolutions in residual blocks. Afterwards, grouped convolutions become popular in efficient CNNs design due to their properties of lower parameter and computational cost, such as CondenseNet (Huang et al. 2018) and our HCGNets. It is widely known that DenseNet has a certain redundancy, thus a typical practice is sparsification. SparseNet (Zhu et al. 2018) regularly conducts a sparse rather than full aggregation of previous outputs for each layer, which changes the number of connections from linear to be logarithmic in the overall topology. Learned group convolutions are adopted in CondenseNet to automatically prune unimportant channels for the incoming feature map based on channel-wise L1-norm. However, excessive sparsification affects the superiority of collective learning. Thus we only decrease the number of modules but retain dense connectivity to reduce redundancy, which is empirically more effective than sparsification.

Combinations of ResNet and DenseNet. To enjoy the advantages and avoid drawbacks of both two connectivities, many combinations have proposed. DPN (Chen et al. 2017) adopts dual path architectures, which can facilitate effective

feature reuse by residual path and feature exploration by dense path in parallel. MixNet (Wang et al. 2018a) blends two connectivity to implement feature aggregation with more flexible positions and sizes, further ResNet, DenseNet and DPN can be treated as particular cases of MixNet. Recently proposed AOGNet (Li, Song, and Wu 2019) utilizes AND-OR Grammar to generate CNNs by parsing feature map as a sentence, where AND-node denotes channel-wise concatenation and OR-node denotes element-wise addition. It demonstrates that the compositional and hierarchical aggregation in AOGNet is more effective than cascade-based way in DPN. Moreover, addition and concatenation as the meta-operations are also widely applied in the field of neural architecture search, such as NASNet (Zoph et al. 2018), PNASNet (Liu et al. 2018) and AmoebaNet (Real et al. 2019). Extensive experiments indicates that the nested way for feature aggregation in our HCGNet perform the best.

Attention Mechanisms Attention has been widely applied in a range of tasks, from machine translation (Bahdanau, Cho, and Bengio 2014) and is later extended to computer vision, e.g., image classification (Wang et al. 2017). SENet (Hu, Shen, and Sun 2018) introduces a lightweight gate to capture channel-wise dependencies for rescaling channel features. SKNet (Li et al. 2019) further employs a dynamic kernel selection attention for weighted fusion multi-scale features inspired by InceptionNets (Szegedy et al. 2017). Beyond channel, CBAM (Woo et al. 2018) also constructs a spatial attention map to recalibrate spatial features. To capture long-range dependency, GCNet (Cao et al. 2019) simplifies non-local block (Wang et al. 2018b) to implement query-independent context modeling based on single branch information. Differ them in roles or mechanisms, we build a forget gate to capture channel-wise dependency for decaying the reused feature, while an update gate fully models the global context features from multi-scale information.

Revisiting ResNet and DenseNet

We revisit the classical ResNet and DenseNet with their individual residual connectivity and dense connectivity, and further investigate their mechanisms of parameter sharing and feature learning. Finally, we analyse the overall efficiency of ResNet and DenseNet.

Parameter Sharing

Residual connectivity implicitly accompanies a parameter sharing mechanism between the reused features and newly extracted features. We now formally describe why the parameter sharing mechanism can take place in residual connectivity but not in dense connectivity. Concretely, we draw upon \mathcal{F} to denote the bottleneck unit. Consider the input feature-map $\mathbf{x}_{l-1} \in \mathbb{R}^{H \times W \times C}$ to the l -th residual block, corresponding transformation is as following:

$$\mathbf{x}_l = \mathbf{x}_{l-1} + \mathcal{F}_l(\mathbf{x}_{l-1}; W_l) = \mathbf{x}_{l-1} + \tilde{\mathbf{x}}_l \quad (1)$$

Where \mathbf{x}_{l-1} can be considered as the reused feature map, W_l and $\mathcal{F}_l(\mathbf{x}_{l-1}; W_l)$ refer to convolutional weights and newly

extracted feature map, respectively. $\tilde{\mathbf{x}}_l \in \mathbb{R}^{H \times W \times C}$ represents $\mathcal{F}_l(\mathbf{x}_{l-1}; W_l)$ for simplicity. Afterwards, \mathbf{x}_l becomes a new input for the next residual block to proceed the transformation:

$$\begin{aligned}\mathbf{x}_{l+1} &= \mathbf{x}_l + \mathcal{F}_{l+1}(\mathbf{x}_l; W_{l+1}) \\ &= \mathbf{x}_l + \mathcal{F}_{l+1}(\tilde{\mathbf{x}}_l + \mathbf{x}_{l-1}; W_{l+1}) \\ &= \mathbf{x}_l + \mathcal{F}_{l+1}(\tilde{\mathbf{x}}_l; W_{l+1}) + \mathcal{F}_{l+1}(\mathbf{x}_{l-1}; W_{l+1})\end{aligned}\quad (2)$$

In the $l+1$ -th residual block, \mathbf{x}_{l-1} and $\tilde{\mathbf{x}}_l$ are shared with the same W_{l+1} and operations. Similar analysis about dense connectivity is exhibited as follows. Output of the l -th module in dense connectivity is the concatenation of input $\mathbf{x}_{l-1} \in \mathbb{R}^{H \times W \times C}$ and newly extracted feature map $\tilde{\mathbf{x}}_l \in \mathbb{R}^{H \times W \times \tilde{C}}$ along the channels:

$$\mathbf{x}_l = \mathbf{x}_{l-1} \parallel \mathcal{F}_l(\mathbf{x}_{l-1}; W_l) = \mathbf{x}_{l-1} \parallel \tilde{\mathbf{x}}_l \quad (3)$$

Then, the next module receives \mathbf{x}_l and conducts the following transformation:

$$\begin{aligned}\mathbf{x}_{l+1} &= \mathbf{x}_l \parallel \mathcal{F}_{l+1}(\mathbf{x}_l; W_{l+1}) \\ &= \mathbf{x}_l \parallel \mathcal{F}_{l+1}([\mathbf{x}_{l-1} \parallel \tilde{\mathbf{x}}_l]; [W_{l+1}^{(1)} \parallel W_{l+1}^{(2)}]) \\ &= \mathbf{x}_l \parallel [\mathcal{F}_{l+1}(\mathbf{x}_{l-1}; W_{l+1}^{(1)}) + \mathcal{F}_{l+1}(\tilde{\mathbf{x}}_l; W_{l+1}^{(2)})]\end{aligned}\quad (4)$$

Where $W_{l+1}^{(1)}$ and $W_{l+1}^{(2)}$ denote the different convolutional weights for acting on the reused feature map \mathbf{x}_{l-1} and newly extracted feature map $\tilde{\mathbf{x}}_l$, respectively.

Feature Learning

The final output of residual block is the element-wise summation of input and newly extracted feature map. This summation pattern facilitates efficient feature reuse without increasing the size of feature map thus reducing parameter redundancy. But one potential fact is that too many aggregation by summation may collapse the feature representation and thus impede the information flow, hence some early informative features may be lost inevitably. Furthermore, parameter sharing mechanism damages the capability of exploring new features.

Subsequently proposed DenseNet develop a global dense connectivity, where the output feature-map of each preceding module flows to the all subsequent modules directly. Different from the element-wise summation, input and newly extracted feature maps are combined by concatenation along the channels. As a consequence, dense connectivity is capable of transferring the early feature-maps to later modules, which preserves the all preceding feature information and facilitate the full exploitation of existing features. Moreover, various modules with different weights conduct a collective learning for the same features, which can promote effective feature exploration.

Overall Efficiency

It is widely known that DenseNet-100 with 0.8M parameters slightly outperforms ResNet-1001 with 10.2M parameters on CIFAR10 dataset. The explicit parameter gap is that DenseNet-100 is quite shallower than ResNet-1001 due to

the more effective feature exploitation and exploration produced by collective learning, while ResNet mainly depends on increase depth to improve the representational power of features. Empirically, DenseNet can also have extremely few number of filters in each convolutional layer due to the collective learning mechanism that further improve the efficiency.

However, one potential weakness of dense connectivity is the redundancy of repeated extraction with the same features. Under this connectivity pattern, early features flow to all subsequent layers, even if they have few contributions. By contrast, residual connectivity has a relatively low redundancy due to the parameter sharing mechanism.

Networks Architecture

Hybrid Connectivity Pattern

To take advantages and weaken faults of both dense and residual connectivity, we develop a hybrid connectivity pattern, which can enjoy the effective feature learning and few filters of each module from global dense connectivity as well as efficient feature reuse by parameter sharing from local residual connectivity. Figure 1 illustrates this pattern within the hybrid block schematically. Note that hybrid connectivity pattern exists in the hybrid block which consists of n ($n \geq 1$) modules. Match to the definition of growth rate in DenseNet, each module produces one feature map with k channels. The basic module consists of two cells, which we call them as cell 1 and cell 2, respectively. Globally, input of each module is a concatenation of all feature-maps produced by preceding modules and transferred by dense connectivity. Locally, residual connectivity provide a shortcut that allows the output of cell 1 bypassing cell 2 and being added to the new features generated by cell 2 to form the output.

Instantiation of Basic Module

To orchestrate our hybrid connectivity, we design a basic SMG module which includes a squeeze cell, a multi-scale excitation cell and gate mechanisms. Unless specified otherwise, each convolution is bound a pre-activation, which refers to the three consecutive operations: batch normalization (BN)-rectified linear unit (ReLU)-Conv.

Squeeze cell. This cell which locates at the beginning of SMG module is responsible for generating the compact feature map from input to improve parameter and computational efficiency for subsequent processing. 1×1 convolution is firstly adopted for reducing the number of input channels \tilde{C} to $\lfloor \alpha \cdot C \rfloor$, where $\alpha \in (1, +\infty)$ can be reckoned as a width multiplier, and C denotes the number of final output channels of squeeze cell. Then, 3×3 grouped convolution (GConv) with g groups proceeds to squeeze the feature map by reducing the number of channels from $\alpha \cdot C$ to C . Furthermore, it can also play a down-sampling of 3×3 kernel by a stride S of 2. To summarize, the number of channels are gradually decreased by a shape of inverted pyramid: $\tilde{C} \rightarrow \alpha \cdot C \rightarrow C$.

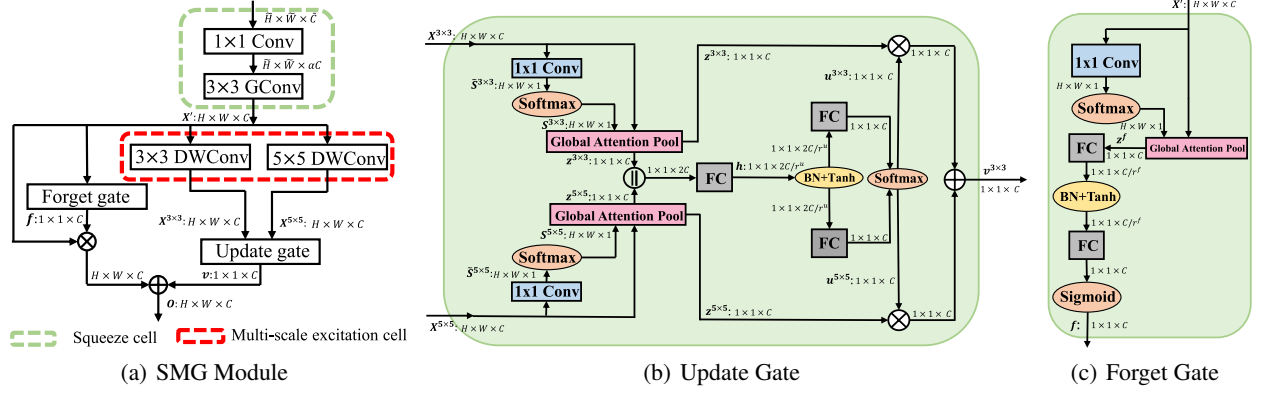


Figure 2: Illustrations of SMG module, update gate and forget gate. In all figures, \oplus and \otimes denote broadcast element-wise addition and multiplication, respectively. We employ feature dimensions to describe the flow of feature maps for better understanding. Note that spatial size $\tilde{H} \times \tilde{W} \neq H \times W$ only if stride $S = 2$ of 3×3 GConv in Fig.2(a).

Multi-scale excitation cell. Squeezed feature map enters this cell for multi-scale excitation by multi-branch convolutions with different kernel sizes. Note that the cost of parameter and computation is extremely cheap because of the few input channels, and the size of feature map throughout this cell is unchanged. To further improve efficiency, we adopt 3×3 and 5×5 depthwise convolutions (DWConv) with 1 and 2 paddings, respectively. Moreover, dilation convolution with a kernel size of 3×3 and a dilation size of 2 is used to approximate 5×5 kernel for better trade-off between efficiency and performance. The output of this cell is two-branch feature maps produced by 3×3 and 5×5 DWConv, respectively.

Update gate. To capture long-range dependency, we utilize update gate to model the global context features from multi-scale information. Figure 2(b) shows the overall details about the update gate, which can be sequentially summarized for 2 stages: spatial attention and channel attention.

spatial attention: We perform a global context modeling for calculating spatial-wise weights of each position. For the given feature map $\mathbf{X}^{3 \times 3} \in \mathbb{R}^{H \times W \times C}$, a 1×1 convolutional filter shrinks it along channel dimensions to a spatial attention map $\tilde{\mathbf{S}}^{3 \times 3} \in \mathbb{R}^{H \times W \times 1}$, an then a softmax function normalizes it to obtain the final spatial attention map $\mathbf{S}^{3 \times 3} \in \mathbb{R}^{H \times W \times 1}$:

$$\mathbf{S}_{i,j,1}^{3 \times 3} = \frac{e^{\tilde{\mathbf{S}}_{i,j,1}^{3 \times 3}}}{\sum_{x=1}^H \sum_{y=1}^W e^{\tilde{\mathbf{S}}_{x,y,1}^{3 \times 3}}} \quad (5)$$

We employ global attention pooling via weighted averaging with $\mathbf{S}^{3 \times 3}$ to shrink the global spatial information and generate the global context feature map $\mathbf{z}^{3 \times 3} \in \mathbb{R}^{1 \times 1 \times C}$. The c -th channel of $\mathbf{z}^{3 \times 3}$ is as follows:

$$\mathbf{z}_c^{3 \times 3} = \sum_{x=1}^H \sum_{y=1}^W \mathbf{X}_{x,y,c}^{3 \times 3} * \mathbf{S}_{x,y,1}^{3 \times 3} \quad (6)$$

Here, $*$ denotes element multiplication. Based on the above framework, $\mathbf{z}^{5 \times 5} \in \mathbb{R}^{1 \times 1 \times C}$ can also be obtained by input feature map $\mathbf{X}^{5 \times 5} \in \mathbb{R}^{H \times W \times C}$.

channel attention: To maintain the integrity of information, we concatenate $\mathbf{z}^{3 \times 3}$ and $\mathbf{z}^{5 \times 5}$ as the input. Then it is transformed to a hidden representation $\mathbf{h} \in \mathbb{R}^{1 \times 1 \times 2 \times C / r^u}$, which is always a compact feature by setting a reduction ratio r^u for better efficiency. This is achieved by a fully connected (FC) layer with non-linearity:

$$\mathbf{h} = \tanh(\text{BN}(\mathbf{W}[\mathbf{z}^{3 \times 3}, \mathbf{z}^{5 \times 5}]) + \mathbf{b}) \quad (7)$$

Where BN is the batch normalization, $\mathbf{W} \in \mathbb{R}^{2 \times C \times 2 \times C / r^u}$ and $\mathbf{b} \in \mathbb{R}^{2 \times C / r^u}$ denotes the weight and bias of FC layer.

It is noteworthy that we adopt tanh rather than ReLU as our non-linearity function. For the one side, ReLU inevitably destroys feature representational power especially in low-dimensional space to a great extent, while tanh preserves information by a softer way. For the other side, although it is widely known that tanh is more prone to cause gradient vanish as the increasing depth of CNN, this problem could not occur in our HCGNets because of the hybrid connectivity that can significantly strength the gradient back-propagation. Experimental evidence also proves that tanh is more effective than ReLU in our HCGNets.

Two-branch FC layers act on fusion representation \mathbf{h} to generate two intermediate channel attention maps $\tilde{\mathbf{u}}^{3 \times 3} \in \mathbb{R}^{1 \times 1 \times C}$ and $\tilde{\mathbf{u}}^{5 \times 5} \in \mathbb{R}^{1 \times 1 \times C}$:

$$\tilde{\mathbf{u}}^{3 \times 3} = \mathbf{W}^{3 \times 3} \mathbf{h} + \mathbf{b}^{3 \times 3}, \tilde{\mathbf{u}}^{5 \times 5} = \mathbf{W}^{5 \times 5} \mathbf{h} + \mathbf{b}^{5 \times 3} \quad (8)$$

Where $\mathbf{W}^{3 \times 3}, \mathbf{W}^{5 \times 5} \in \mathbb{R}^{2 \times C / r \times C}$ and $\mathbf{b}^{3 \times 3}, \mathbf{b}^{5 \times 5} \in \mathbb{R}^C$ denotes the weights and biases of two FC layers. Then a simple softmax function conducts a normalization between $\tilde{\mathbf{u}}^{3 \times 3}$ and $\tilde{\mathbf{u}}^{5 \times 5}$ to produce the two final channel attention maps $\mathbf{u}^{3 \times 3} \in \mathbb{R}^{1 \times 1 \times C}$ and $\mathbf{u}^{5 \times 5} \in \mathbb{R}^{1 \times 1 \times C}$:

$$\mathbf{u}^{3 \times 3} = \frac{e^{\tilde{\mathbf{u}}^{3 \times 3}}}{e^{\tilde{\mathbf{u}}^{3 \times 3}} + e^{\tilde{\mathbf{u}}^{5 \times 5}}}, \mathbf{u}^{5 \times 5} = \frac{e^{\tilde{\mathbf{u}}^{5 \times 5}}}{e^{\tilde{\mathbf{u}}^{3 \times 3}} + e^{\tilde{\mathbf{u}}^{5 \times 5}}} \quad (9)$$

$\mathbf{u}^{3 \times 3}$ and $\mathbf{u}^{5 \times 5}$ can be regarded as the proportions of aggregating multi-scale global context features, weighted fusion of which is the output of update gate:

$$\mathbf{v}_c = \mathbf{u}_c^{3 \times 3} \cdot \mathbf{z}_c^{3 \times 3} + \mathbf{u}_c^{5 \times 5} \cdot \mathbf{z}_c^{5 \times 5}, \mathbf{u}_c^{3 \times 3} + \mathbf{u}_c^{5 \times 5} = 1 \quad (10)$$

Where \mathbf{v}_c is the c -th channel of the output $\mathbf{v} \in \mathbb{R}^{1 \times 1 \times C}$.

Forget Gate. To decay the reused feature map by channel-wise weights, we locate a forget gate (see Fig.2(c)) on the residual connection before information fusion. It can also be sequentially summarized for 2 stages: spatial attention and channel attention.

spatial attention: For the given feature map $\mathbf{X}' \in \mathbb{R}^{H \times W \times C}$, we perform the global attention pooling as same as update gate, thus a channel descriptor $\mathbf{z}^f \in \mathbb{R}^{1 \times 1 \times C}$ can be obtained.

channel attention: To meet the requirement of weighted decay for each channel, the final output of each channel weight should be within $(0, 1)$, thus we refer SE block, which stacks two continuous FC layers as a bottleneck and terminated by sigmoid function. Differ SE block, we insert a batch normalization layer for ease optimization and replace ReLU with tanh as our non-linearity. In short, the sequent transformations are as follows for the input \mathbf{z}^f :

$$\mathbf{f} = \sigma(\mathbf{W}_2^f(\tanh(\mathbf{BN}(\mathbf{W}_1^f \mathbf{z}^f + \mathbf{b}_1^f))) + \mathbf{b}_2^f) \quad (11)$$

Where σ is the sigmoid function, $\mathbf{W}_1^f \in \mathbb{R}^{C \times C/r^f}$, $\mathbf{b}_1^f \in \mathbb{R}^{C/r^f}$, $\mathbf{W}_2^f \in \mathbb{R}^{C/r^f \times C}$ and $\mathbf{b}_2^f \in \mathbb{R}^C$. r^f is the bottleneck ratio and $\mathbf{f} \in \mathbb{R}^{1 \times 1 \times C}$ is the final channel attention map.

Information fusion. For any given feature map entering SMG module, squeeze cell firstly condenses it to a compact feature map denoted by \mathbf{X}' . Then \mathbf{X}' enters multi-scale excitation cell and generate two-branch outputs $\mathbf{X}^{3 \times 3}$ and $\mathbf{X}^{5 \times 5}$ by 3×3 and 5×5 DWConvs, respectively. Since then, \mathbf{X}' can be regarded as the reused features, while $\mathbf{X}^{3 \times 3}$ and $\mathbf{X}^{5 \times 5}$ are the newly extracted features. An update gate integrates $\mathbf{X}^{3 \times 3}$ and $\mathbf{X}^{5 \times 5}$ to model a global context feature map \mathbf{v} and we aggregate it to the decayed \mathbf{X}' of each position by addition to build the final output $\mathbf{O} \in \mathbb{R}^{H \times W \times C}$. It can be observed that we maintain the magnitude of new features unchanged while decay that of old features, which can facilitate the effective feature exploration, meanwhile retain the capability of feature re-exploitation to some extent.

Macro-architecture.

Macro-architecture of our HCGNet is quite similar with DenseNet, where the main different is that the original dense blocks are replaced with our hybrid blocks. At the begining of HCGNet is a stem, which is a composite function to process the initial input images. Then multiple hybrid blocks are stacked with various spatial stage. Between two contiguous hybrid blocks, we adopt a transition layer to perform down-sampling and connectivity truncation, whose role is match to DenseNet. After the final hybrid block, a global average pooling attached with a softmax classifier calculates the probabilities of various categories.

Both hybrid block and transition layer adopt SMG modules but with different hyperparameter settings. We only stack one SMG module to build each transition layer and a compression factor $\theta = 0.5$ is utilized to reduce the number of channels, i.e., $C = \theta \tilde{C}$. For each SMG module, we set $g = 4$, $\alpha = 4$ and $r^u = r^f = 2$ in hybrid blocks, while set $g = 1$, $\alpha = 1.5$, $S = 2$ and $r^u = r^f = 4$ in transition layers. Note that we apply the standard convolutions

Table 1: HCGNet-(3,6,12,8)-(k=32,48,64,96)(A) network architecture for ImageNet-1k classification. Each row describes stage, modules information and input resolution.

Stage	Module	Resolution
Stem	$[3 \times 3 \text{ Conv-BN-ReLU}] \times 3$	224×224
	$3 \times 3 \text{ max pool}$	112×112
Hybrid Block	SMG $\times 3$ ($k = 32$)	56×56
Transition	SMG $\times 1$	56×56
Hybrid Block	SMG $\times 6$ ($k = 48$)	28×28
Transition	SMG $\times 1$	28×28
Hybrid Block	SMG $\times 12$ ($k = 64$)	14×14
Transition	SMG $\times 1$	14×14
Hybrid Block	SMG $\times 8$ ($k = 96$)	7×7
Classification	global average pool	1×1
	1000D FC, softmax	-

in transition layers for best capability of feature extraction and grouped convolutions in dense blocks for better trade-off between efficiency and performance. Compared with the dense block, we set less multiplier α and larger reduction ratio r^u , r^f for better efficiency due to the more channels of feature map in transition layers.

Specifically, we construct several networks to act on the image classification across the CIFAR and ImageNet datasets. For CIFAR, we adopt a 3×3 standard convolution with stride 1 as the stem that the number of output channels is twice the growth rate of the first dense block. And we build three networks with various model specifications: HCGNet-(8,8,8)-(k=12,24,36), HCGNet-(8,8,8)-(k=24,36,64) and HCGNet-(12,12,12)-(k=36,48,80). Formally, the first m -tuple indicates that there are m dense blocks, where each figure denotes the number of SMG modules in the corresponding dense block. The second m -tuple denotes m growth rates of m dense blocks, respectively. For ImageNet, the stem consists of three contiguous 3×3 Conv-BN-ReLU layers (stride 2 for the first layer) with 32, 32, 64 output channels, and attached by a 3×3 max pooling with stride 2. We construct three networks: HCGNet-(3,6,12,8)-(k=32,48,64,96)(A, see Table 1), HCGNet-(4,8,14,10)-(k=48,56,72,112)(B), HCGNet-(6,12,18,14)-(k=48,56,72,112)(C).

Experiments

Experiments on CIFAR

Dataset. Both CIFAR-10 and CIFAR-100 datasets comprise 50k training images and 10k test images corresponding to 10 and 100 classes, respectively. We apply a standard data augmentation strategy following (Huang et al. 2017). Note that we don't employ any other augmentations like cutout (DeVries and Taylor 2017) so as to be consistent with previous works. Finally, each image is normalized using channel-wise means and standard deviations.

Training details and analysis. We employ a stochastic gradient descent (SGD) optimizer with a Nesterov momen-

Table 2: Comparison of our HCGNet against state-of-the-art networks about test error rate (%) across CIFAR-10 and CIFAR-100 datasets. Note that the first and second blocks contain human-designed and auto-searched architectures, respectively.

Type	Model	Params	CIFAR-10	CIFAR-100
Human	CondenseNet-182 (Huang et al. 2018)	4.2M	3.76	18.47
	SparseNet-BC (Zhu et al. 2018)	16.7M	4.10	18.22
	AOGNet (Li, Song, and Wu 2019)	15.8M	3.42	16.93
	DenseNet-BC-190 (Huang et al. 2017)	25.6M	3.46	17.18
	DPN-28-10 (Chen et al. 2017)	47.8M	3.65	20.23
	MixNet-190 (Wang et al. 2018a)	48.5M	3.13	16.96
Auto	PNASNet (Liu et al. 2018)	3.2M	3.41	19.53
	NASNet-A (Zoph et al. 2018)	3.3M	3.41	19.70
	ENASNet (Pham et al. 2018)	4.6M	3.54	19.43
	AmoebaNet-A (Real et al. 2019)	4.6M	3.34	-
	AmoebaNet-B (Real et al. 2019)	34.9M	2.98	17.66
	NASNet-A (Zoph et al. 2018)+Cutout	50.9M	-	16.03
	ENAS (Pham et al. 2018)+Cutout	52.7M	-	16.44
	PNAS (Liu et al. 2018)+Cutout	53.0M	-	16.70
Human(ours)	HCGNet-(8,8,8)-(k=12,24,36)	1.1M	3.15	18.13
	HCGNet-(8,8,8)-(k=24,36,64)	3.1M	2.29	16.54
	HCGNet-(12,12,12)-(k=36,48,80)	11.4M	2.14	15.96

tum of 0.9 and a batch size of 128. Training are regularized by a weight decay of $1e-4$ and mixup with $\alpha = 1$ (Zhang et al. 2017). For HCGNet-1.1M, we train it for 1270 epochs using a cosine learning rate curve with initial learning rate of 0.1, $T_0 = 10$, $T_{mul} = 2$ following (Loshchilov and Hutter 2016). For HCGNet>1.1M, we train them for 1260 epochs including two continuous 630 epochs, each of them is a cosine learning rate curve with initial learning rate of 0.1, $T_0 = 10$, $T_{mul} = 2$. It can be observed that we employ more frequent warm restarts for the large networks to improve the capability of global optimization because the larger search space would lead to more deceptive points. Moreover, we add a dropblock layer (Ghiasi, Lin, and Le 2018) after each transition layer with a dynamic drop rate within $(0, 0.1)$, where drop rate = $0.1 - \text{learning rate}$.

Comparison with human-designed networks. DenseNet-190 has 31 modules in each dense block, while HCGNet-3.1M with 8 modules in each hybrid block thus reduces 93% redundancy but with substantial accuracy gains. Moreover, HCGNet-3.1M significantly outperforms other sparsification variants, such as SparseNet and CondenseNet, which indicates that our optimization of DenseNet is more effective than sparsification method. HCGNet-3.1M using $15\times$ fewer parameters surpasses MixNet-190, which represents the most generalization form of ResNet and DenseNet. It also uses $5\times$ fewer parameters but obtains better result than concurrent AOGNet consistently, which is the state-of-the-art human network by hierarchical and compositional feature integration. Consequently, our nested integration is the best method among other combinations and variants of ResNet and DenseNet.

Comparison with auto-searched networks. Notably, our HCGNets are also more efficient than auto-searched net-

Table 3: Comparison of our HCGNets against popular networks about top-1 test error rate (%) across the reduced ImageNet. Note that we will report the final results on the full ImageNet in the future version.

Model	Params	FLOPs	Top-1
MixNet-105	11.2M	5.0G	17.13
MixNet-121	21.9M	8.3G	16.22
MixNet-141	41.1M	13.1G	15.44
DPN-68	12.8M	2.5G	17.21
DPN-92	38.0M	6.5G	15.71
DPN-98	61.6M	11.7G	15.11
DenseNet-169	14.2M	3.5G	17.55
DenseNet-201	20.0M	4.4G	16.53
DenseNet-264	33.4M	6.0G	15.68
SparseNet-201	14.9M	9.2G	16.67
ResNet-50	25.6M	3.9G	18.32
ResNet-50+SE	28.1M	3.9G	17.02
ResNet-50+CBAM	28.1M	3.9G	16.71
ResNet-101	44.6M	7.6G	17.18
ResNet-101+SE	49.3M	7.6G	16.50
ResNet-101+CBAM	49.3M	7.6G	15.92
ResNeXt-50	25.0M	3.8G	16.55
ResNeXt-50+SE	27.6M	3.8G	16.13
ResNeXt-50+CBAM	27.6M	3.8G	16.15
ResNeXt-101	44.2M	7.5G	15.96
ResNeXt-101+SE	49.0M	7.5G	15.72
ResNeXt-101+CBAM	49.0M	7.5G	15.53
HCGNet-A	12.9M	2.0G	16.48
HCGNet-B	22.4M	4.0G	15.66
HCGNet-C	40.0M	7.1G	14.95

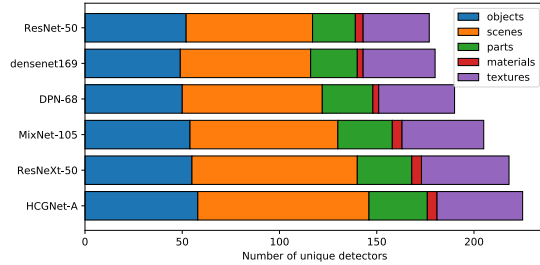


Figure 3: Comparison of interpretability by network dissection (Bau et al. 2017) based on ImageNet pretrained models.

works. Compared with other networks with small setting, HCGNet-3.1M achieves $>1\%$ and $>3\%$ reductions on CIFAR-10 and CIFAR-100 error rates, respectively. Additionally, it is noteworthy that HCGNet-1.1M can also obtain superior performance with unprecedented efficiency. For large setting, HCGNet-11.4M generally reduces parameters by an order of magnitude but achieves the best results. Somewhat surprisingly, HCGNet-11M can outperform the most competitive NASNet-A with only 22% parameters.

Experiments on ImageNet 2012

Dataset. ImageNet 2012 dataset comprises 1.2 million training images and 50k validation images corresponding to 1000 classes. Due to time limitation, we adopt a reduced subset of the original ImageNet with 100 classes (randomly chosen) to conduct our experiments. We employ the data augmentation following (Huang et al. 2017) and (Cubuk et al. 2018). Final error rates are reported by single-crop with size 224×224 at test time on the validation set.

Training details. We employ a SGD optimizer with a Nesterov momentum of 0.9 on 2 GPUs (NVIDIA V100). The batch size is 256 (128 per GPU). Training are regularized by a weight decay of $4e-5$, label smoothing with $\epsilon = 0.1$ (Szegedy et al. 2016) and mixup with $\alpha = 0.4$. All networks are trained for 90 epochs using a cosine learning rate curve from 0.1 to 0 gradually. For HCGNets, We add a drop-block layer after each transition layer and a dynamic drop rate= $0.1 \cdot \text{learning rate}$.

Comparison with popular networks. As shown in Table 3, our HCGNets perform the best compared with all other models with less or comparable complexity in terms of top-1 error rate. It is noteworthy that DenseNet-169 stacks 4 dense blocks with 6,12,32,32 modules, while HCGNet-A utilizes shallower design with 3,6,12,8 modules for 4 hybrid blocks, thus reducing 88% redundancy but obtaining above absolute 1.1% gain of performance. Furthermore, HCGNets yields significantly better results than the families of DenseNet, MixNet and DPN under comparable complexity. Remarkably, using considerable $4.6\times$ fewer FLOPs, HCGNet-A can also slightly surpass SparseNet-201, which is the state-of-the-art variant of DenseNet. The family of HCGNet can consistently obtain better performance than the families of ResNet, ResNeXt and their attention-based variants, which represent the widely applied models in practice.

Table 4: Results of HCGNet-A with various combinations of g and α .

g	α	Params	FLOPs	Top-1
1	2.5	12.0M	2.2G	17.10
2	3	11.3M	2.0G	16.80
4	4	11.7M	2.0G	16.48
8	4.5	11.7M	2.0G	16.58

Table 5: Results of HCGNet-A with various components ablation. R,F,U denote the components of residual connectivity, forget gate and update gate, respectively.

Component	Params	FLOPs	Top-1
baseline	11.7M	2.0G	16.48
−F	11.4M	2.0G	16.63
−U	10.6M	2.0G	17.12
−RFU	10.3M	2.0G	17.33

Model interpretability. We quantify the interpretability by network dissection metric, which compares the number of unique detectors in the final convolutional layer. Figure 3 shows that our HCGNet obtain the highest score, which demonstrates that the designs of hybrid connectivity and SMG module can generate the best latent representations.

Ablation Study

Group number g . g is a crucial element for better trade-off between efficiency and performance in hybrid blocks. To study its effect, we vary g to 1,2,4,8 gradually while increasing width multiplier α to maintain the similar parameters and FLOPs for a fair comparison. From Table 4, we can observe that $g = 4$ and $\alpha = 4$ are preferred for best trade-off.

Component ablation. We investigate the effectiveness of three components in SMG module: residual connectivity, forget gate and update gate. Note that ablating residual connectivity can also lead to the disappearance of both forget and update gates. Without update gate, the output of the multi-scale excitation cell is the element-wise addition $\mathbf{X}^{3 \times 3}$ and $\mathbf{X}^{5 \times 5}$. From Table 5, we can observe that each component is indispensable but only introduces negligible parameters and FLOPs.

Conclusion.

This paper develops an efficient architecture with the innovative designs of macro-connectivity and micro-module. Moreover, we also construct attention-based forget gate and update gate to assist feature learning. Extensive experiments on CIFAR and ImageNet demonstrate that our HCGNets achieve better performance than state-of-the-art networks with less or comparable complexity. We hope our HCGNets may inspire the future study of architectural design and search.

References

- Bahdanau, D.; Cho, K.; and Bengio, Y. 2014. Neural machine translation by jointly learning to align and translate. *arXiv preprint arXiv:1409.0473*.
- Bau, D.; Zhou, B.; Khosla, A.; Oliva, A.; and Torralba, A. 2017. Network dissection: Quantifying interpretability of deep visual representations. In *Proceedings of the IEEE Conference on Computer Vision and Pattern Recognition*, 6541–6549.
- Cao, Y.; Xu, J.; Lin, S.; Wei, F.; and Hu, H. 2019. Gcnet: Non-local networks meet squeeze-excitation networks and beyond. *arXiv preprint arXiv:1904.11492*.
- Chen, Y.; Li, J.; Xiao, H.; Jin, X.; Yan, S.; and Feng, J. 2017. Dual path networks. In *Advances in Neural Information Processing Systems*, 4467–4475.
- Cubuk, E. D.; Zoph, B.; Mane, D.; Vasudevan, V.; and Le, Q. V. 2018. Autoaugment: Learning augmentation policies from data. *arXiv preprint arXiv:1805.09501*.
- Deng, J.; Dong, W.; Socher, R.; Li, L.-J.; Li, K.; and Fei-Fei, L. 2009. Imagenet: A large-scale hierarchical image database. In *2009 IEEE conference on computer vision and pattern recognition*, 248–255. Ieee.
- DeVries, T., and Taylor, G. W. 2017. Improved regularization of convolutional neural networks with cutout. *arXiv preprint arXiv:1708.04552*.
- Ghiasi, G.; Lin, T.-Y.; and Le, Q. V. 2018. Dropblock: A regularization method for convolutional networks. In *Advances in Neural Information Processing Systems*, 10727–10737.
- He, K.; Zhang, X.; Ren, S.; and Sun, J. 2016. Deep residual learning for image recognition. In *Proceedings of the IEEE conference on computer vision and pattern recognition*, 770–778.
- Hu, J.; Shen, L.; and Sun, G. 2018. Squeeze-and-excitation networks. In *Proceedings of the IEEE conference on computer vision and pattern recognition*, 7132–7141.
- Huang, G.; Liu, Z.; Van Der Maaten, L.; and Weinberger, K. Q. 2017. Densely connected convolutional networks. In *Proceedings of the IEEE conference on computer vision and pattern recognition*, 4700–4708.
- Huang, G.; Liu, S.; Van der Maaten, L.; and Weinberger, K. Q. 2018. Condensenet: An efficient densenet using learned group convolutions. In *Proceedings of the IEEE Conference on Computer Vision and Pattern Recognition*, 2752–2761.
- Krizhevsky, A., and Hinton, G. 2009. Learning multiple layers of features from tiny images. Technical report, Citeseer.
- Li, X.; Wang, W.; Hu, X.; and Yang, J. 2019. Selective kernel networks. In *Proceedings of the IEEE conference on computer vision and pattern recognition*.
- Li, X.; Song, X.; and Wu, T. 2019. Aognets: Compositional grammatical architectures for deep learning. In *IEEE Conference on Computer Vision and Pattern Recognition, CVPR*.
- Liu, C.; Zoph, B.; Neumann, M.; Shlens, J.; Hua, W.; Li, L.-J.; Fei-Fei, L.; Yuille, A.; Huang, J.; and Murphy, K. 2018. Progressive neural architecture search. In *Proceedings of the European Conference on Computer Vision (ECCV)*, 19–34.
- Loshchilov, I., and Hutter, F. 2016. Sgdr: Stochastic gradient descent with warm restarts. *arXiv preprint arXiv:1608.03983*.
- Pham, H.; Guan, M. Y.; Zoph, B.; Le, Q. V.; and Dean, J. 2018. Efficient neural architecture search via parameter sharing. *arXiv preprint arXiv:1802.03268*.
- Real, E.; Aggarwal, A.; Huang, Y.; and Le, Q. V. 2019. Regularized evolution for image classifier architecture search. In *Proceedings of the AAAI Conference on Artificial Intelligence*, volume 33, 4780–4789.
- Szegedy, C.; Vanhoucke, V.; Ioffe, S.; Shlens, J.; and Wojna, Z. 2016. Rethinking the inception architecture for computer vision. In *Proceedings of the IEEE conference on computer vision and pattern recognition*, 2818–2826.
- Szegedy, C.; Ioffe, S.; Vanhoucke, V.; and Alemi, A. A. 2017. Inception-v4, inception-resnet and the impact of residual connections on learning. In *Thirty-First AAAI Conference on Artificial Intelligence*.
- Wang, F.; Jiang, M.; Qian, C.; Yang, S.; Li, C.; Zhang, H.; Wang, X.; and Tang, X. 2017. Residual attention network for image classification. In *Proceedings of the IEEE Conference on Computer Vision and Pattern Recognition*, 3156–3164.
- Wang, W.; Li, X.; Yang, J.; and Lu, T. 2018a. Mixed link networks. *arXiv preprint arXiv:1802.01808*.
- Wang, X.; Girshick, R.; Gupta, A.; and He, K. 2018b. Non-local neural networks. In *Proceedings of the IEEE Conference on Computer Vision and Pattern Recognition*, 7794–7803.
- Woo, S.; Park, J.; Lee, J.-Y.; and So Kweon, I. 2018. Cbam: Convolutional block attention module. In *Proceedings of the European Conference on Computer Vision (ECCV)*, 3–19.
- Xie, S.; Girshick, R.; Dollár, P.; Tu, Z.; and He, K. 2017. Aggregated residual transformations for deep neural networks. In *Proceedings of the IEEE conference on computer vision and pattern recognition*, 1492–1500.
- Zhang, H.; Cisse, M.; Dauphin, Y. N.; and Lopez-Paz, D. 2017. mixup: Beyond empirical risk minimization. *arXiv preprint arXiv:1710.09412*.
- Zhu, L.; Deng, R.; Maire, M.; Deng, Z.; Mori, G.; and Tan, P. 2018. Sparsely aggregated convolutional networks. In *Proceedings of the European Conference on Computer Vision (ECCV)*, 186–201.
- Zoph, B.; Vasudevan, V.; Shlens, J.; and Le, Q. V. 2018. Learning transferable architectures for scalable image recognition. In *Proceedings of the IEEE conference on computer vision and pattern recognition*, 8697–8710.